Synthesis and Characterization of $Ni_{0.5}Cu_{0.5}Cr_2O_4$ Nanostructure for Discoloration of Aniline Dye under Visible Light from Wastewater

Soleimani, Fatemeh; Salehi, Mehdi *+

Department of Chemistry, Semnan University, Semnan 35351-19111, I.R. IRAN

Gholizadeh, Ahmad

School of Physics, Damghan University (DU), Damghan, I.R. IRAN

ABSTRACT: *In this research, pure-phased $Ni_{0.5}Cu_{0.5}Cr_2O_4$ synthesis via solid-state method successfully. In the other part, the photocatalytic activity of synthesized $Ni_{0.5}Cu_{0.5}Cr_2O_4$ was investigated in various aspects by using Malachite green as a pollutant and compared with the number of previous photocatalysts. The Photocatalysis process is a promising technique for solving many current environmental and energy issues. The environmental pollutant, especially water contaminates, can influence human health, animals, and the ecosystem. Dye as one of the most important pollutants has investigated in this study. In this study, purification and crystal structure of material have been determined by X-Ray powder Diffraction (XRD) method. The results showed that the synthesized $Ni_{0.5}Cu_{0.5}Cr_2O_4$ was crystallized in tetragonal structure with space group I 41/AMD. The morphology of obtained materials was modified by Field Emission Scanning Electron Microscope (FESEM). Also, the material was characterized by Fourier-Transform InfraRed (FT-IR) spectroscopy and Thermo Gravimetric Analysis (TGA).*

KEYWORDS: *$Ni_{0.5}Cu_{0.5}Cr_2O_4$; Photocatalytic activity; Solid-state; Malachite green.*

INTRODUCTION

Spinel-type metal oxides with general formula AB_2O_4 have attracted increasing attention due to their various applications like optical, electrical, magnetic, and catalytic properties [1, 2]. There are two types of cations in normal spinel structure, A^{2+} and B^{3+}, which A^{2+} ions occupy tetrahedral sites and B^{3+} ions occupy octahedral sites [3]. Copper chromite is one of these normal spinel metal oxides with c/a <1 (where a and c are lattice constants in a unit cell along the x- and z-axes respectively) [4]. This chromite can be used as a versatile catalyst for the oxidation of CO which is wildly used in space launch vehicles [5] and catalyzed hydrogenation process in oil industries [6, 7]. In the other side, studying magnetic properties of copper chromite reviled that it has ferromagnetic property in some cases and paramagnetic property in some other cases, even though the number of

** To whom correspondence should be addressed.*
+ E-mail: msalehi@semnan.ac.ir
1021-9986/2020/2/11-19 9/$/5.09

studies show that it is ferrimagnetic [8, 9]. Also, $CuCr_2O_4$ is a p-type semiconductor which has been widely studied as photocatalyst, and its 1.4ev band gape make it highly activated under visible light [10, 11].

The most common methods which have been used for synthesizing copper chromite are: hydrothermal [6], co-precipitation [12, 13], sol-gel [14], thermal decomposition [15], solid state [11] and so on. In this study, ceramic synthesis or solid-state has been used, as solventless techniques which need high reaction temperature to diffuse of ions.

$Ni_{0.5}Cu_{0.5}Cr_2O_4$ is the chromite which has been considered in this study, in which Ni^{+2} and Cu^{2+} occupy tetrahedral sites contemporaneously. This chromite has been synthesized via solid state method [8, 16] which is used in this study. There are other researches that some properties of this chromite were compared; for example, the catalyzed burning rate of ammonium perchlorate and polystyrene solid composite caparison shew that $Ni_{0.5}Cu_{0.5}Cr_2O_4$ has better performance than $CuCr_2O_4$ [16]. Also, these two chromite doesn't have any specific difference in magnetic properties [8].

The contamination of water is an important issue which has been tried to eliminate them to the pacification of water in recent years [17]. The concentration and type of these pollutants mainly change due to the function of the demands of manufacturing [18]. There are various methods that have been developed to remove textile dyes like; chemical oxidation technology[19], adsorption [20], photocatalysis [21] and so on.

Toxic dyes are perpetually left in the industrial waste waters. As a result of their aromatic structures, the photodegradation of them is significant [20]. The pollutant which is assessed in this study is malachite green (MG), a toxic cationic triphenylmethane dye that is widely used in food coloring, textile, and ceramics industry.

In the present work, the effect of doping Ni^{2+} in the spinel structure of $CuCr_2O_4$ has been investigated. In the first step, the pure phased $Ni_{0.5}Cu_{0.5}Cr_2O_4$ is synthesized successfully. In the next step, it is tried to assess the photocatalytic activity of $Ni_{0.5}Cu_{0.5}Cr_2O_4$ for degradation of an aniline dye (malachite green) with the assistance of H_2O_2.

EXPERIMENTAL SECTION

Materials and methods

All chemicals were of analytical grade, obtained from commercial sources (Merck company), used without further purification. Also, the MG or *N*-[4-[[4-(dimethylamino) phenyl] phenylmethylene]-2,5-cyclohexadien-1-ylidene]-*N*-methyl-oxalate, was prepared from Merck and its structure is presented in Fig. 1. Phase identifications were performed on a powder X-ray diffractometer D5000 (Siemens AG, Munich, Germany) using CuKα radiation in the range 2θ =10-90° and the XRD data was analyzed by using X'Pert package and Fullprof program. The morphology of the obtained materials was examined with a field emission scanning electron microscope (Hitachi FE-SEM model S-4160). FT-IR spectra were recorded on a Tensor 27 (Bruker Corporation, Germany) in the range 400-4000 cm^{-1}. The thermogravimetric analysis (TGA) has been recorded by STA PT 1600 thermal analysis performed between 25-800°C with the 5°C/min constant rate of heating under the air atmosphere in alumina pan. For controlling photodegradation of Malachite green is used UV–vis diffuse reflectance spectra which were recorded by UV-Visible spectra (Shimadzu UV-1650 PC).

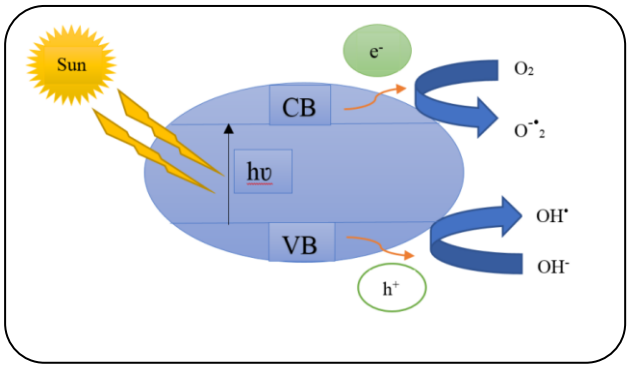

Scheme 1: Mechanism of photocatalytic activity

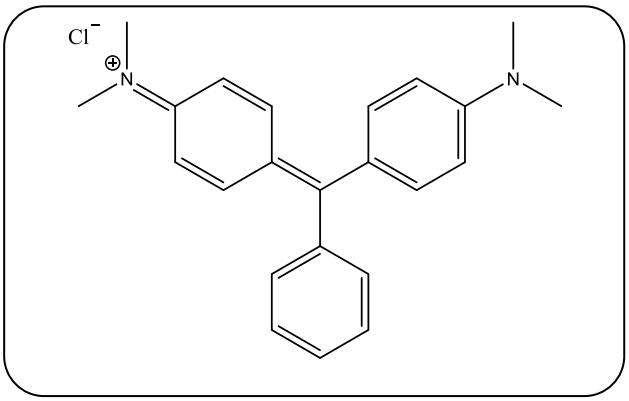

Fig. 1: Chemical structure of malachite green.

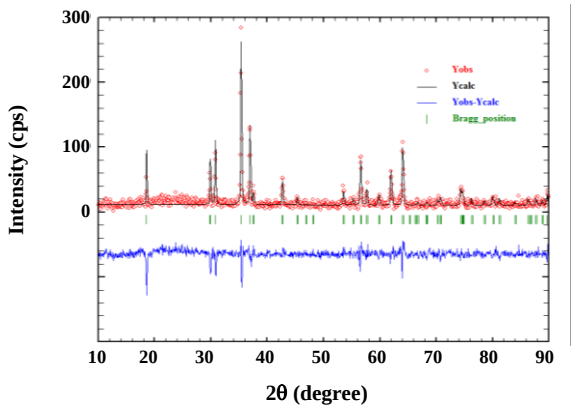

Fig. 2: Calculated PXRD pattern for Rietveld profile of synthesized $Ni_{0.5}Cu_{0.5}Cr_2O_4$

Synthesis of $Ni_{0.5}Cu_{0.5}Cr_2O_4$

In this method, at first 0.5 mmol $Cu(NO_3)_2$ and 0.5 mmol of $Ni(NO_3)_2$ and 2 mmol $Cr(NO_3)_2$ were added to platinum crucibles and heated in a furnace maintained at 900°C for 8 h. After the final heat treatment, it was cooled to room temperature at a rate of 2°/min. The obtained $Ni_{0.5}Cu_{0.5}Cr_2O_4$ was collected**.**

RESULTS AND DISCUSSION

PXRD analysis

The XRD diffraction pattern of synthesized $Ni_{0.5}Cu_{0.5}Cr_2O_4$ is presented in Fig. 2. The investigation of XRD data has been done by X'Pert High Score package and Fullprof program [22]. Identification of structure and crystal information confirms the formation of single phase $Ni_{0.5}Cu_{0.5}Cr_2O_4$. The results demonstrate that all the diffraction peaks of $Ni_{0.5}Cu_{0.5}Cr_2O_4$ can be quite well indexed in tetragonal structure (space group I 41/A M D) and the best fit with the least difference is carried out (Fig. 2). Complete adaptability and perfect performance in Rietveld refinement require the best amount of initial values and type of space group, which are taken from X'Pert package. The refined lattice parameters are: $a = b = 5.9879$ and $c = 7.9958$.

The crystallite size of particles can be calculated by Scherrer's equation [23]

$$D = 0.94\lambda/(\beta\cos\theta) \quad (1)$$

In this equation, D show particle size, λ is X-ray wavelength (0.154 nm) and, β is broadening at half the maximum intensity of the peak. The largest peak is located at 35.3572°. The obtained average crystallite size of the synthesized $Ni_{0.5}Cu_{0.5}Cr_2O_4$ nanoparticle is 44.51nm.

Morphological analysis

For studying the morphology and the sizes of the synthesized material, FE-SEM was used. Fig. 3 shows various magnificent of Nickle copper chromite. This figure demonstrates micro multi-dimensional particles that the approximate size of them is about 250 nm.

ThermoGravimetric Analysis (TGA) analysis

ThermoGravimetric Analysis (TGA)/ Differential Thermal Analysis (DTA) is a method which is used for determining characteristics of the material by gaining weight as a result of increasing temperature. Fig. 4 shows the TGA and DTA analysis of synthesized $Ni_{0.5}Cu_{0.5}Cr_2O_4$. The TGA has two important sections, the first part is related to dehydration of physically absorption water that belongs to less than 200°C, and after that its weight loss is less than 10% up to 800°C.

Fourier Transform InfraRed (FT-IR) spectroscopy analysis

FT-IR spectra of as-prepared $Ni_{0.5}Cu_{0.5}Cr_2O_4$ with the wave number range 400-4000 cm^{-1} is observed in Fig. 5. There is a peak located at 3153 cm^{-1} that is attributed to O-H bond stretching. Also, the peak located at 1660 cm^{-1} refers to bond bending of H_2O. Two sharp peaks at 613cm^{-1} and 501 cm^{-1} corresponding to Ni-O stretching bond, Ni-O and Cu-O vibration bond [24, 25]. Also, these two sharp vibration bands demonstrate the lattice vibrations of tetragonal in spinel structure.

UV-vis diffuse reflectance analysis

The band gap energy (E_g) of $Ni_{0.5}Cu_{0.5}Cr_2O_4$ is determined by Tauc model which is used in semiconductor material commonly [26]

$$(\alpha h\upsilon)^{1/r} = A(h\upsilon - E_g) \quad (4)$$

Which α is linear absorption coefficient of the material; h is Plank's constant; υ is photon's frequency; A is proportionally constant; E_g is band gap energy. The value of exponent (r) depends on forbidden or allowed electron transition that causes to create 4 stats: directly allowed transition (r = 1/2), directly forbidden transition (r = 3/2), indirectly allowed transition (r = 2), indirectly

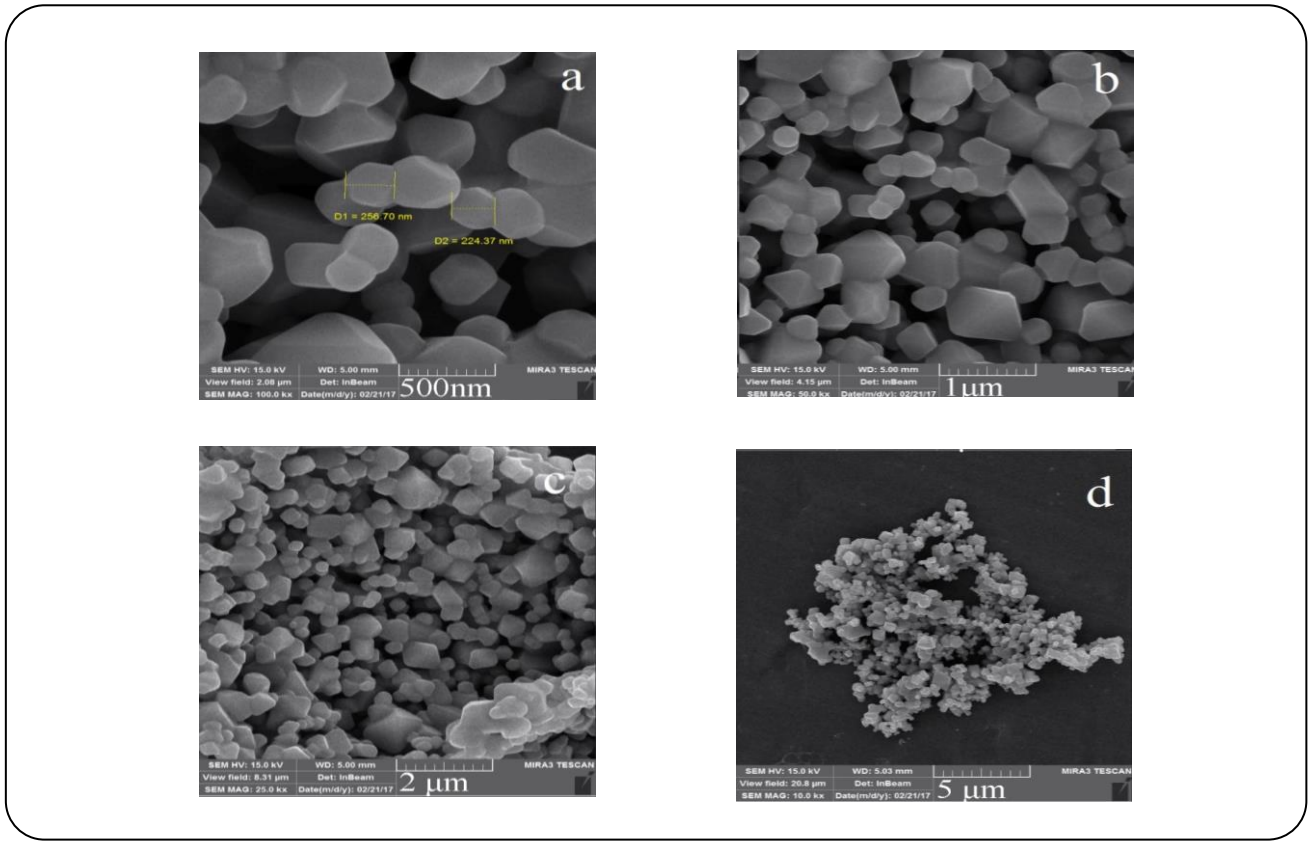

Fig. 3: FESEM images of the hydrothermally synthesized $Ni_{0.5}Cu_{0.5}Cr_2O_4$ nanomaterials.

forbidden transition (r = 3). The value of Direct band gap energy can be calculated by using the $(\alpha h\upsilon)^2$ versus $h\upsilon$ plot and extrapolating a straight line on a curve with the x-axis. According to the UV-vis diffuse reflectance analysis, the band gap of synthesized $Ni_{0.5}Cu_{0.5}Cr_2O_4$ is about 1.62 eV. It means that the narrow band gap doesn't need high energetic light sources for photocatalytic degradation, so that the irradiation would be done by visible light.

Photocatalyst activity of $Ni_{0.5}Cu_{0.5}Cr_2O_4$

The photocatalytic activities of synthesized material were investigated by an Aniline dye pollutant -Malachite green- under 5 FPL 36W 70LM and room temperature.

Effect of catalyst concentration

Obee and Hay's studies shew that the higher initial catalyst concentration leads to increasing the reaction rate of a reaction like photooxidation of ethylene [27, 28]. Also, many other research proofed them, but Cao's research shew that this enhancement has occurred up to the specific initial amount of catalyst [29]; for example, in photo-oxidation of ethylene, the reaction rate wasn't increased when the initial concentration of 1-butene was higher than 7 ppm.

The effect of catalyst dosage on photodegradation of MG has been investigated in this part. Fig. 7 demonstrates the kinetic data diagram of different amount of $Ni_{0.5}Cu_{0.5}Cr_2O_4$ on the rate of photo-degradation. It is found that the reaction rate has been increased up to 0.02g of catalyst, after that the reaction rate remains stable. The possible reason for increasing photo-degradation efficiency by adding the mass of catalyst can be justified that the higher amount of catalyst leads to more transformation of electrons and better separation of electrons-holes. Fig. 8 shows the linear changes of LnC_0/C_t versus time that confirm the first-order reaction. the rate constants for 0.005g, 0.01g, 0.02g, 0.03g and 0.04g of $Ni_{0.5}Cu_{0.5}Cr_2O_4$ are 0.1947, 0.2258, 0.2812, 0.3034 and .3044 min^{-1}, respectively. The last two numbers confirm the stable condition of the reaction. Also, Fig. 9 shows the

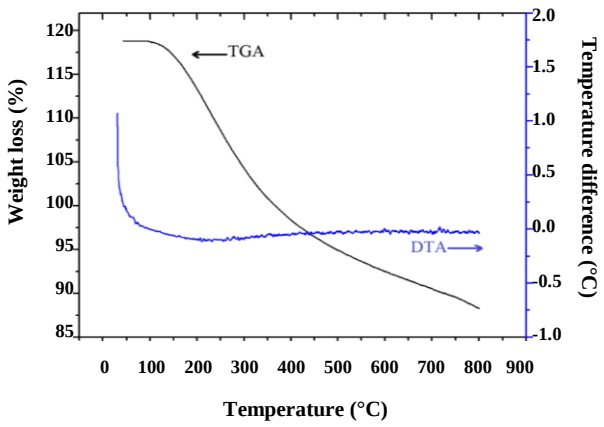

Fig. 4: Black: TGA. Blue: DTA pattern of $Ni_{0.5}Cu_{0.5}Cr_2O_4$.

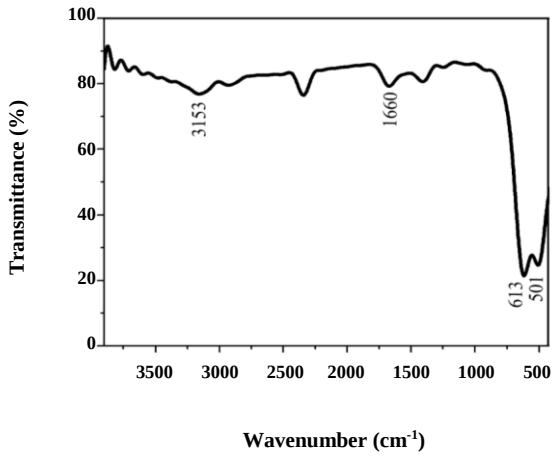

Fig. 5: FT-IR spectra of $Ni_{0.5}Cu_{0.5}Cr_2O_4$.

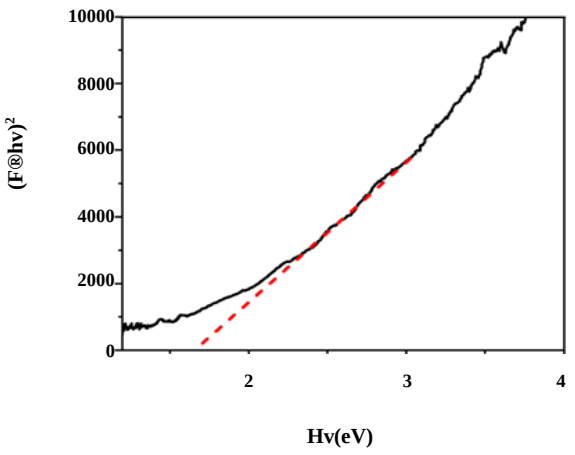

Fig. 6: $(F(R)hv)^2$ versus (hv) Plot for $Ni_{0.5}Cu_{0.5}Cr_2O_4$.

decrease of the absorption peak of Malachite green at λ=617 nm.

Effect of H_2O_2

The H_2O_2 in the reaction process, convert to hydroxyl radicals. To direct relationship between attending OH• and progressing photooxidative degradation of MG, the various amount of H_2O_2 was added to the solution [30]. According to Fig. 10, this first order kinetic diagram shows that The $Ni_{0.5}Cu_{0.5}Cr_2O_4$ had low rate photocatalytic activity in the absence of H_2O_2. But in the presence of various amount of H_2O_2, the photocatalytic activity is improved. The degradation rate constant is shown in Fig. 11 when the H_2O_2 dosage increased from 0.2 to 0.5 mL, the constant rate increase from 0.0205 to 0.0676 min^{-1}. The additional dosage of H_2O_2, from 0.5mL to 1mL doesn't show a significant increasing in reaction rate and, k is the change from 0.0676 to 0.0771 min^{-1}.

At the last part, the reusability of this metal oxide was investigated in five cycles. Reusability of the catalysts is one of the most important factors to make it as a useful economical catalyst. So, checking the recyclability is a significant test. High photocatalytic activity of $Ni_{0.5}Cu_{0.5}Cr_2O_4$ leads to high recyclability which is shewn in Fig. 12. The yield of the product approximately didn't change a lot -that was more than 90% after five times, that is an emphasis on its recyclability without lacking obvious activity.

The photocatalytic activity of $Ni_{0.5}Cu_{0.5}Cr_2O_4$ in decolorization performance of MG is compared with other metal oxide. As it's seen, this nano metal oxide has high efficiency rather than the others.

CONCLUSIONS

The of $Ni_{0.5}Cu_{0.5}Cr_2O_4$ nano-scale metal oxide has been successfully synthesized by solid-state method. The multi-dimensions morphology obtain from this process. This sample is used for photodegradation of an aniline dye -MG-. All data of photocatalytic activity were studied by the Langmuir-Hinshelwood pseudo first-order kinetic model and compared with other metal oxide. The synthesized $Ni_{0.5}Cu_{0.5}Cr_2O_4$ had reasonable photodegradation ability as compared with other metal oxides.

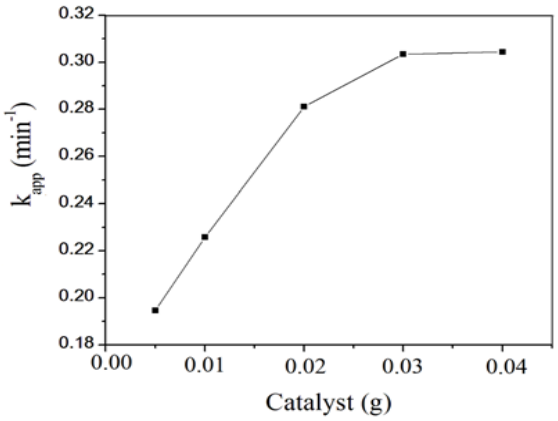

Fig. 7: Kinetics data of photocatalytic degradation of MG on $Ni_{0.5}Cu_{0.5}Cr_2O_4$ in the various amount of catalyst. Dye concentration= 10 mg/L, T=298K.

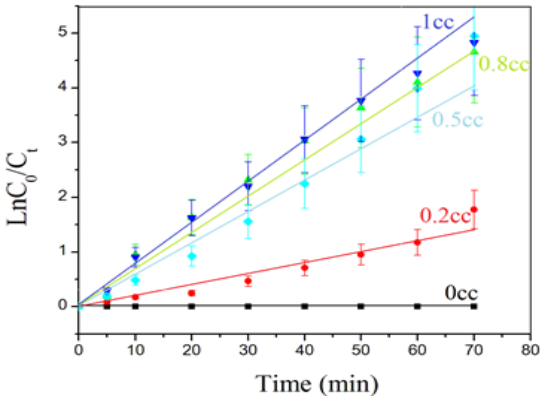

Fig. 10: ***Photocatalytic degradation of MG under visible-light irradiation on $Ni_{0.5}Cu_{0.5}Cr_2O_4$ with different dosages of H_2O_2.***

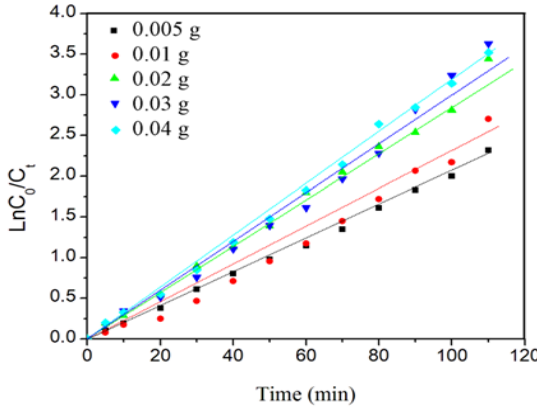

Fig. 8: Photodegradation of MG on $Ni_{0.5}Cu_{0.5}Cr_2O_4$ under visible light irradiation at different catalyst values, Dye concentration= 10 mg/L, T=298K.

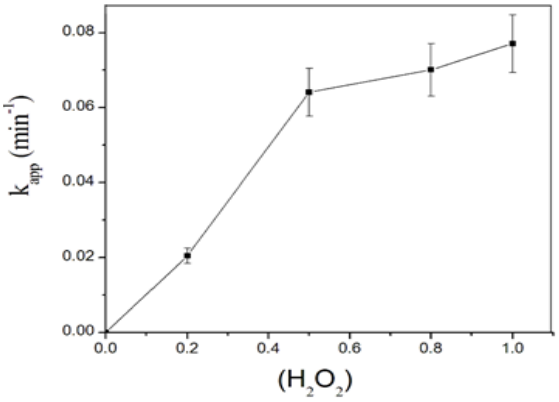

Fig. 11: Kinetics data of photocatalytic degradation of MG on $Ni_{0.5}Cu_{0.5}Cr_2O_4$ with different dosages of H_2O_2. Dye concentration= 10 mg/L, T=298K.

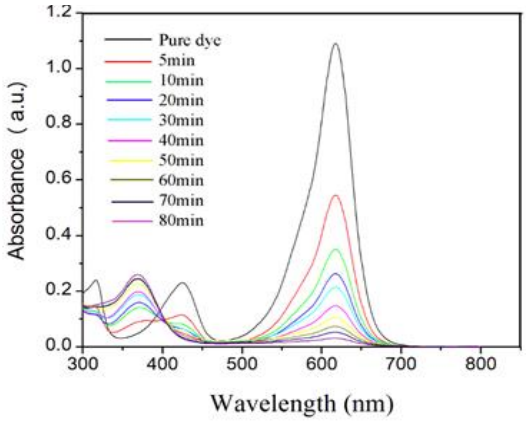

Fig. 9: Absorption spectra of MG by using $Ni_{0.5}Cu_{0.5}Cr_2O_4$ (10 mg) at different times in the presence of H_2O_2 under visible light irradiation.

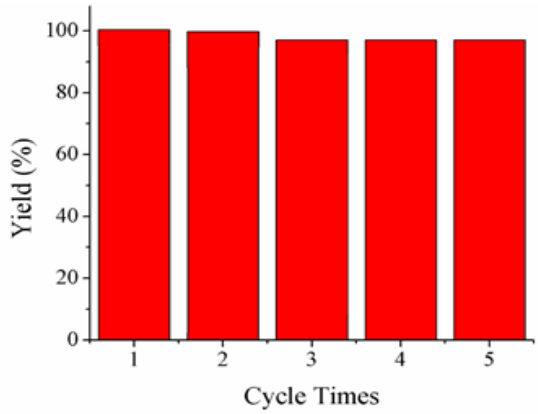

Fig. 12: reusability of $Ni_{0.5}Cu_{0.5}Cr_2O_4$ in degradation of .MG.

Table 1: Comparison aspect of the photocatalytic degradation of the $Ni_{0.5}Cu_{0.5}Cr_2O_4$ with other metal oxide.

Catalyst	time	Catalyst suspension (g) in 100mL sol	Efficiency	ref
$Ni_{0.5}Cu_{0.5}Cr_2O_4$	80	0.03	100	This work
Pd/WO_3	180	0.015	50%	[31]
Fe_2O_3@SBA	60	0.35	69%	[32]
$Fe_{0.01}Ni_{0.01}Zn_{0.98}O$/PAM	240	25	92.13%	[33]
$BiWO_6$	75	0.01	100%	[34]
TiO_2/WO_3	30	0.01	99%	[35]
Fe_2O_3/SnO_2	360	0.02	86	[36]

Acknowledgments

The authors gratefully thank Semnan University for supporting this study.

Received : Feb. 17, 2018 ; Accepted : Oct. 24, 2018

REFERENCES

[1] Gholizadeh A., A Comparative Study of Physical Properties in Fe_3O_4 Nanoparticles Prepared by Coprecipitation and Citrate Methods, *J Am Ceram Soc.*, **100**: 3577-3588 (2017)

[2] Gholizadeh A., A Comparative Study of the Physical Properties of Cu-Zn Ferrites Annealed under Different Atmospheres and Temperatures: Magnetic Enhancement of $Cu_{0.5}Zn_{0.5}Fe_2O_4$ Nanoparticles by a Reducing Atmosphere, *J. Magn. Magn. Mater.*, **452**: 389-397 (2018)

[3] Shamgani N., Gholizadeh A., Structural, Magnetic and Elastic Properties of $Mn_{0.3-x}MgxCu_{0.2}Zn_{0.5}Fe_3O_4$ Nanoparticles, *Ceram. Int.* (2018)

[4] Paul B., Bhuyan B., Purkayastha D.D., Dhar S.S., Behera S., Facile Synthesis of Spinel $CuCr_2O_4$ Nanoparticles and Studies of their Photocatalytic Activity in Degradation of some Selected Organic Dyes, *J. Alloys. Compd.*, **648**: 629-635 (2015).

[5] Prasad R., Singh P., Prasad R., Singh P., A Review on CO Oxidation Over Copper Chromite Catalyst, *Catal. Rev.*, **54**: 224-279 (2012).

[6] Acharyya S.S., Ghosh S., Bal R., Catalytic Oxidation of Aniline to Azoxybenzene Over $CuCr_2O_4$ Spinel Nanoparticle Catalyst, *ACS Sustain. Chem. Eng.*, **2**: 584-589 (2014).

[7] Lian C., Ren F., Liu Y., Zhao G., Ji Y., Rong H., Jia W., Ma L., Lu H., Wang D., Heterogeneous Selective Hydrogenation of Ethylene Carbonate to Methanol and Ethylene Glycol over a Copper Chromite Nanocatalyst, *Chem. Commun.*, **51**: 1252-1254 (2015).

[8] Dubey B., Nath N., Tiwari B., Tripathi A., , Magnetic Properties of $Ni_{1-x}Cu_xCr_2O_4(0\leqslant x\leqslant 1)$ Compounds, *Bull. Mater. Sci.*, **5**: 153-161 (1983).

[9] Gurgel T.T., Buzinaro M., Moreno N., Magnetization Study in $CuCr_2O_4$ Spinel Oxide, *J. Supercond. Nov. Magn.*, **26**: 2557-2559 (2013).

[10] Dollase W., O'Neill H.S.C., The Spinels $CuCr_2O_4$ and $CuRh_2O_4$, *Acta. Crystallogr C Struct. Chem.*, **53**: 657-659 (1997).

[11] Boumaza S., Bouarab R., Trari M., Bouguelia A., Hydrogen Photo-Evolution over the Spinel $CuCr_2O_4$, *Energy Convers. Manag.*, **50**: 62-68 (2009).

[12] Premalatha K., Raghavan P., Viswanathan B., Liquid Phase Oxidation of Benzyl Alcohol with Molecular Oxygen Catalyzed by Metal Chromites, *Appl. Catal., A*, **419**: 203-209 (2012).

[13] Beshkar F., Amiri O., Salavati-Niasari M., Beshkar F., Novel Dendrite-like $CuCr_2O_4$ Photocatalyst Prepared by a Simple Route in order to Remove of Azo Dye in Textile and Dyeing Wastewater, *J. Mater. Sci.: Materials in Electronics*, **26**: 8182-8192 (2015).

[14] Xiao Z., Xiu J., Wang X., Zhang B., Williams C.T., Su D., Liang C., Controlled Preparation and Characterization of Supported $CuCr_2O_4$ Catalysts for Hydrogenolysis of Highly Concentrated Glycerol, *Catal. Sci. Technol.*, **3**: 1108-1115 (2013).

[15] Geng Q., Zhao X., Gao X., Yang S., Liu G., Low-Temperature Combustion Synthesis of $CuCr_2O_4$ Spinel Powder for Spectrally Selective Paints, *J. Sol Gel Sci. Technol.*, **61**: 281-288 (2012).

[16] Dubey B., Nath N., Tripathi A., Tiwari N., Catalysed Combustion of Ammonium Perchlorate, Polystyrene and Their Composite Propellants, *Indian Journal of Engineering & Material Science*, **1**: 341-349 (1994).

[17] Yola M.L., Eren T., Atar N., Wang S., Adsorptive and Photocatalytic Removal of Reactive Dyes by Silver Nanoparticle-Colemanite ore Waste, *Chem. Eng. J.*, **242**: 333-340 (2014).

[18] Yola M.L., Eren T., Atar N., A Novel Efficient Photocatalyst Based on TiO_2 Nanoparticles Involved Boron Enrichment Waste for Photocatalytic Degradation of Atrazine, *Chem. Eng. J*, **250**: 288-294 (2014).

[19] Palanichamy M., Palanisamy P.N., Baskar R., Sakthisharmila P., Sivakumar P., A Comparative Study on the Competitiveness of Photo-Assisted Chemical Oxidation (PACO) with Electrocoagulation (EC) for the Effective Decolorization of Reactive Blue Dye, *Iran. J. Chem. Chem. Eng. (IJCCE)*, **36**: 71-85 (2017).

[20] Gupta V.K., Agarwal S., Olgun A., Demir H.İ., Yola M.L., Atar N., Adsorptive Properties of Molasses Modified Boron Enrichment Waste Based Nanoclay for Removal of Basic Dyes, *Ind. Eng. Chem. Res.*, **34**: 244-249 (2016).

[21] Malekhosseini, H., Mahanpoor K., Khosravi M., Motiee F., Kinetic Modeling and Photocatalytic Reactor Designed for Removal of Resorcinol in Water by Nano $ZnFe_2O_4$/Copper Slag as Catalyst: Using Full Factorial Design of Experiment, *Iran. J. Chem Chem. Eng. (IJCCE)*, **39**(3): 257-266 (2019).

[22] Rodrigueg-Carvajal J., Leon L, Brillounin, "Gifsuryvette, A Program for Rietveld, Profile Matching and Integrated Intensity Refinements for X-Ray and Neutron Data", Version 1.6. Laboratorie Leon, Brillounin, Gifsuryvette, France, (2009).

[23] Gholizadeh A., Jafari E., Effects of Sintering Atmosphere and Temperature on Structural and Magnetic Properties of Ni-Cu-Zn Ferrite Nano-Particles: Magnetic Enhancement by a Reducing Atmosphere, *J. Magn. Magn. Mater*, **422**: 328-336 (2017) .

[24] Rahdar A., Aliahmad M., Azizi Y., NiO Nanoparticles: Synthesis and Characterization, *J. Nanostruct*, **5**: 145-151 (2015).

[25] Radhakrishnan A.A., Beena B.B., Structural and Optical Absorption Analysis of CuO Nanoparticles, *Ind. J. Adv. Chem. Sci.*, **2**: 158-161 (2014).

[26] Gholizadeh A., Tajabor N., Influence of N_2- and Ar-Ambient Annealing on the Physical Properties of SnO_2:Co Transparent Conducting Films, *Mat. Sci. Semicon. Proc.*, **13**: 162-166, (2010).

[27] Obee T.N., Hay S.O., Effects of Moisture and Temperature on the Photooxidation of Ethylene on Titania, *Environ. Sci. Technol.*, **31**: 2034-2038 (1997).

[28] Gnanaprakasam, A.J., Sivakumar, V.M., Thirumarimurugan, M., Investigation of Photocatalytic Activity of Nd-Doped ZnO Nanoparticles Using Brilliant Green Dye: Synthesis and Characterization, *Iran. J. Chem. Chem. Eng. (IJCCE)*, **37**(2): 61-71 (2018).

[29] Cao L., Huang A., Spiess F.-J., Suib S.L., Gas-Phase Oxidation of 1-Butene Using Nanoscale TiO_2 Photocatalysts, *J. Catal.*, **188**: 48-57 (1999).

[30] Tseng D.-H., Juang L.-C., Huang H.-H., Effect of Oxygen and Hydrogen Peroxide on the Photocatalytic Degradation of Monochlorobenzene in Aqueous Suspension, *Int. J. Photoenergy* (2012).

[31] Liu Y., Ohko Y., Zhang R., Yang Y., Zhang Z., Degradation of Malachite Green on Pd/WO_3 Photocatalysts under Simulated Solar Light, *J. Hazard. Mater.*, **184**: 386-391 (2010).

[32] Aliyan H., Fazaeli R., Jalilian R., Fe_3O_4@mesoporous SBA-15: A magnetically recoverable catalyst for photodegradation of malachite green, *Appl. Surf. Sci.*, **276**: 147-153 (2013).

[33] Pitchaimuthu S., Rajalakshmi S., Kannan N., Velusamy P., Enhanced Photocatalytic Activity of Titanium Dioxide by β-Cyclodextrin in Decoloration of Acid Yellow 99 Dye, *Desalin. Water Treat.*, **52**: 3392-3402 (2014).

[34] Yamashita T., Hayes P., Analysis of XPS Spectra of Fe^{2+} and Fe^{3+} Ions in Oxide Materials, *Appl. Surf. Sci.*, **254**: 2441-2449 (2008).

[35] Grosvenor A., Kobe B., Biesinger M., McIntyre N., Investigation of Multiplet Splitting of Fe 2p XPS Spectra and Bonding in Iron Compounds, *Surf. Interface. Anal.*, **36**: 1564-1574 (2004).

[36] Pradhan G.K., Reddy K.H., Parida K.M., Facile Fabrication of Mesoporous α-Fe_2O_3/SnO_2 Nanoheterostructure for Photocatalytic Degradation of Malachite Green, *Catal. Today*, **224**: 171-179 (2014).